Constitutive modelling for strain–hardening alloys during isothermal compression

Wang, Hang; Gao, Pengzhe; Turner, Richard; Chen, Huiming; Qi, Liang; Yang, Bin

DOI:
10.1016/j.mtcomm.2020.101040

Document Version
Peer reviewed version

Citation for published version (Harvard):
Wang, H, Gao, P, Turner, R, Chen, H, Qi, L & Yang, B 2020, 'Constitutive modelling for strain–hardening alloys during isothermal compression: an efficient semi-empirical method coupling the effects of strain, temperature and strain-rate ', *Materials Today Communications*, vol. 24, 101040.
https://doi.org/10.1016/j.mtcomm.2020.101040

Constitutive modelling for strain–hardening alloys during isothermal compression: An efficient semi-empirical method coupling the effects of strain, temperature and strain-rate

Hang Wang[a], Pengzhe Gao[a], Richard Turner[b], Huiming Chen[a], Liang Qi[a], Bin Yang[a]*,

a: College of Materials, Metallurgy and Chemistry, Jiangxi University of Science and Technology, Ganzhou, 341000, Jiangxi, China

b: School of Metallurgy & Materials, University of Birmingham, Birmingham, B15 2TT, United Kingdom

*: yangbin65@126.com

Abstract: Constitutive modelling is of importance for metals and alloys which require hot working to improve their mechanical strength. In the present work, a semi-empirical method has been proposed for alloy systems which experience strain hardening e.g. Cu-Cr based alloys, which is easy to implement. This method is based upon the Arrhenius equation, whereby a new parameter α representing the effective stress is introduced. This methodology allows for the effect of strain on the changing back stress to be taken into account, thus the method considers the coupled effects of strain, temperature and strain rate. The value of parameter α can be fitted using exponential function. Experimental data of flow curves during isothermal compression have been used to verify the present model. Compared to the conventional Arrhenius equation using polynomial fitting, the present model reduces the parameters to be fitted without sacrificing accuracy.

Keywords: Constitutive behaviour; Metallic material; Mechanical testing; Microstructures

1. Introduction

Hot working is one of the most important processing steps for metals and alloys in order to achieve improved mechanical properties. Controlling the processing parameters is critical to gain a better understanding of the behaviours of the alloys during hot deformation, among which flow stress is a key factor. A thorough review of the constitutive modelling for the flow behaviours of metals and alloys divides the models into three categories – i) phenomenological, ii) physical-based, and iii) artificial neural network models[1]. The phenomenological models[2-7] tend to be more efficient, and in fact the classical models for dealing with the flow behaviours consider parameters which lack a physical meaning. One of the major drawbacks of the phenomenological models is that the coupling effects of the strain, temperature and strain-rate have not been fully considered in these models. To reflect the coupling effects, strain and strain-rate compensation is suggested for the most commonly used model, the Arrhenius equation, by introducing a polynomial function of strain to describe various parameters[8]. This provides higher precision when describing the flow stress on the basis of parameters fitting.

After reviewing those literatures using the polynomial functions, it was noted that the flow curves can be characterised in to three typical types: (i) with a steady-state stress value; (ii) with a peak stress value; and (iii) with a gradually increasing stress value. A schematic illustration has been given in Figure 1 to show the three cases.

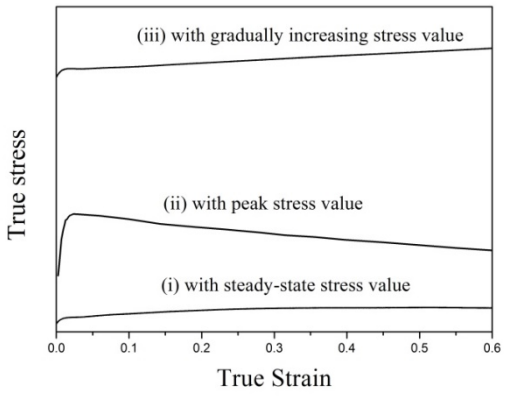

Figure 1: A schematic illustration of the three types of flow curves (i) with steady-state stress value; (ii) with peak stress value; and (iii) with gradually increasing stress value.

(i) To represent flow curves with steady-state stress value such as 10CrMoWNb steel[9] and 9Cr1Mo steel[10], cubic (power of 3) polynomial functions were applied, which led to a correlation coefficient R^2=0.991. For some Al alloys quartic (power of 4) polynomial functions were applied with a good consistency[11-13]. Quartic polynomial functions were successfully applied as well for a Ti alloy[14] and a Cu alloy[15]. A quintic (power of 5) polynomial function was fitted for the X20Cr13 steel[16].

(ii) Flow curves with a peak stress value usually are for Mg[17-19], Ti[20,21], Al[22] alloys and steels[23]. Quintic (power of 5) polynomial functions were used for all these cases, expect AISI420[24]and brass[25] where a hexic (power of 6) polynomial function was applied.

(iii) Flow curves with rising gradually increasing value are a phenomena which can occur in some steels and more commonly in Cu alloys. Quintic (power of 5) and hexic (power of 6) polynomial functions were fitted for steel[26]

and copper alloys[27,28]. In previous work it was shown that only a 7-power heptic polynomial function could fit the curves well for Cu-Cr-In alloys[29].

When considering the literature for all types of flow curves, it is particularly interesting to observe that higher-power polynomial functions are needed for more complex flow curves fitting. This is further evidence of the inferiority of these phenomenological models – and in particular their lack of physical meaning. Nevertheless it is indeed very difficult to obtain a model originated from a physically-based background and which is also easily executed. Therefore, the aim of this present work is to propose a semi-empirical method to improve the Arrhenius equation by defining a parameter reflecting the coupling effect of strain and temperature.

A Cu-Cr based alloy is chosen for investigation for its complexity of strain hardening, precipitation hardening and recovery/re-crystallisation softening during isothermal compression at elevated temperatures. High-strength and high-conductivity copper alloys are widely used in lead frames, track contact lines, and other fields[30-33] Among them, Cu-Cr based alloys have become one of the research hot spots due to their excellent properties. It is generally believed that the high strength of the alloy is caused by small precipitations with typical size being about 10 nm or less[34,35]. During the hot deformation process of Cu-Cr alloy, strain hardening, precipitation hardening, and dynamic recovery, and the softening of dynamic recrystallization are a competitive relationship, which causes the flow stress curve generated during the isothermal compression of the alloy to be very complicated. Therefore, a

corresponding constitutive model is needed to reflect the coupling effects of strain, strain rate, and temperature during the thermal deformation of Cu-Cr alloys.

2. Material and methods

2.1 Sample preparation

Pure copper (99.9 wt.%), Cu-8wt.%Cr, Cu-40wt.%Zr, and pure titanium (99.99 wt.%) were used as raw materials. Ingots (Φ=30 mm) were cast after melting in a medium frequency induction furnace (DS-7-003, Wuxi Doushan). Solution heat treatment was carried out at 950 °C for 1.5 h. Sample bars were cut into size of Φ10 mm × 15 mm for hot deformation.

2.2 Isothermal compression

Isothermal compression tests were performed using a thermomechanical simulator (Gleeble MMS-100) at 700, 750, 800, 850, and 900 °C and strain rates are 0.01, 0.1, 1, and 10 s^{-1}. The sample bars were heated to the correct compression temperature and held for 3 min before compression. The sample bars were compressed by 60% followed by quenching in water at room temperature.

2.3 Microstructure characterisation

Isothermal compression tests were interrupted at three states, with the corresponding true strain being 0.3, 0.6 and 0.9, in order to observe the microstructure evolution during compression. Transmission electron microscopy (TEM, Tecnai-G2-F20, FEI) was used for the microstructure observation, noting especially the dislocation pile-up at each true strain accumulation. X-ray diffraction (XRD, Xpert powder, PANalytical B.V.) was used for phase identification as well as allowing

for an estimation of dislocation density. The estimation method is the so-called Williamson–Hall model[36].

3. Theory

The commonly used Arrhenius equation is expressed as follows,

$$\dot{\varepsilon} = A \cdot f(\sigma) \cdot \exp(-\frac{Q}{RT}) \quad (1)$$

where $\dot{\varepsilon}$ is strain rate; A is a material constant; σ is stress; Q is activation energy; R is the gas constant; and T is temperature. The stress σ is therefore a function of strain rate $\dot{\varepsilon}$ and temperature T – $\sigma = f(\dot{\varepsilon}, T)$. In order to give strain compensation, another contribution term should be added, $\sigma = f(\dot{\varepsilon}, T) f(\varepsilon)$. According to the hyperbolic law,

$$f(\sigma) = [\sinh(\alpha\sigma)]^n \quad (2)$$

those two parameters α and n should be both functions of stress σ which is given as,

$$\alpha = f(\sigma) \quad (3)$$

and

$$n = f(\sigma) \quad (4)$$

During fitting process, it is known that n can be obtained by calculating the slope of $\ln[\sinh(\alpha\sigma)]$ versus $\ln\dot{\varepsilon}$. The value n is dependent on α and thus Equation (4) is not needed. In fact, a careful check of previous work in the literature showed that the value n does not vary a lot for one metal/alloy.

Although a proposed dependency of α on stress σ is presented, it is still not clear which type of function the relationship will take. This is mainly due to the fact that the physical meaning of α remains unclear; and it is assumed that it represents the

percentage of effective stress (by taking off the back stress during different strain stage). It is very difficult to theoretically estimate the effective hardening under the mutual effect of recovery/re-crystallisation softening, strain hardening, and precipitation hardening. As such, the values of α at each corresponding strain accumulation are to be calculated assuming the constant values of activation energy Q and material constant A. The series of values for α and n for different strains are then to be used to fit their relationship function. Using a fitting process (which is given in the following section), the following relationship was obtained;

$$\alpha = \exp(a + b \cdot \varepsilon) \tag{5}$$

and thus a proposed a new constitutive equation is formed,

$$\dot{\varepsilon} = A \cdot \{\sinh[\exp(a + b \cdot \varepsilon) \cdot \sigma]\}^n \cdot \exp(-\frac{Q}{RT}) \tag{6}$$

where a and b are fitting parameters.

4. Results

4.1 Flow curves

Figure 2 shows the flow curves of the Cu-Cr-Zr-Ti alloys compressed at various temperatures and strain rates. It is clear that true stress increases rapidly under the conditions of low temperatures (700 and 750 °C) or high strain rates (1 and 10 s^{-1}) where the strain hardening dominates the flow curve; while the increase of the slope is smallest under the conditions of high temperatures (850 ˚C, 900 ˚C) or low strain rates, where the recovery/re-crystallisation softening effects are competing with the strain hardening.

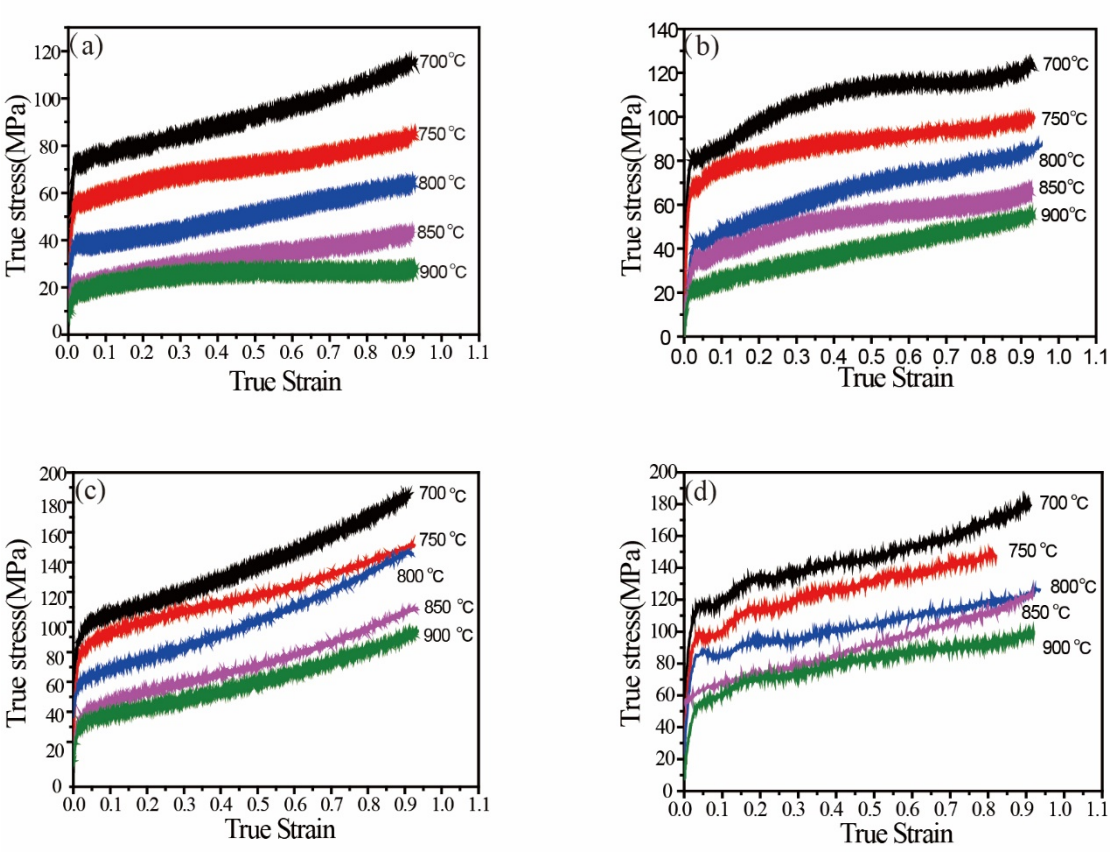

Figure 2: Flow stress curves of the Cu-Cr-Zr-Ti alloys at different strain rates. (a) 0.01 s^{-1}; (b) 0.1 s^{-1}; (c) 1 s^{-1}; (d) 10 s^{-1}.

4.2 Microstructure evolution

Figure 3 shows the microstructure evolution at the desired strain accumulation during isothermal compression (700 °C and 0.01 s^{-1}). Evidence of some dislocations can be observed in Figure 3(a) referring to an intermediate true strain accumulation of 0.3. When the true strain reaches 0.6, more dislocations pile up as shown in Figure 3(b). Finally, severe dislocation accumulation occurs towards the end of compression when the true strain reaches 0.9 in Figure 3(c).

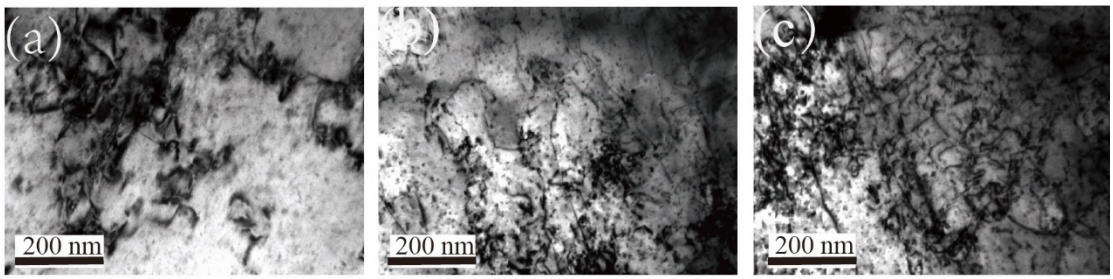

Figure 3: Microstructure of the Cu-Cr-Zr-Ti alloys during isothermal compression (700 °C and 0.01 s^{-1}) using TEM at different strain stages. (a) 0.3; (b) 0.6; (c) 0.9.

Figures 4(a), 4(b) and 4(c) correspond to the three increasing accumulations of true strain of 0.3, 0.6 and 0.9, respectively for the compression condition of 900 °C and 0.01 s^{-1}. No obvious dislocation accumulation or annihilation can be seen in this case.

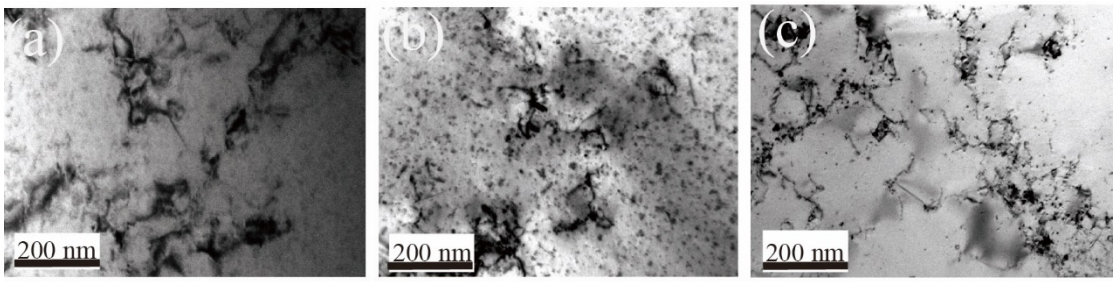

Figure 4: Microstructure of the Cu-Cr-Zr-Ti alloys during isothermal compression (900 °C and 0.01 s^{-1}) using TEM at different strain stages. (a) 0.3; (b) 0.6; (c) 0.9.

XRD patterns are presented in Figure 5 for the samples with true strain of 0.3, 0.6 and 0.9 when compressed at 700 °C and 0.01 s^{-1}. Using the Williamson–Hall model [Williamson and Hall, 1953], dislocation density has been estimated to be 3.8×10^{19} cm^{-2}, 4.5×10^{19} cm^{-2} and 5.4×10^{19} cm^{-2}. The tendency of higher dislocation density at greater strain is consistent with the microstructure evolution as shown in Figure 3.

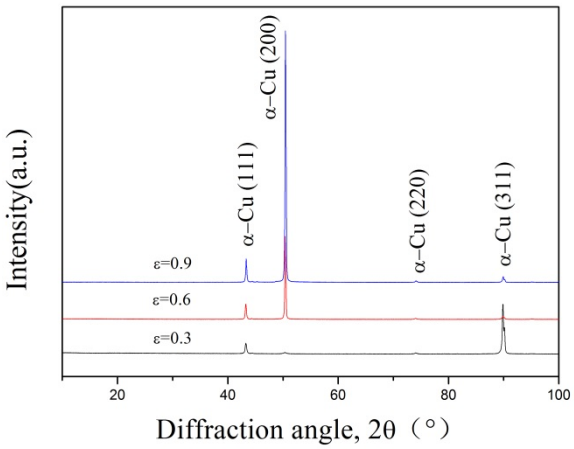

Figure 5: XRD patters of the Cu-Cr-Zr-Ti alloys during isothermal compression (700 °C and 0.01 s^{-1}) using TEM at different strain stages. (a) 0.3; (b) 0.6; (c) 0.9.

4.3 Constitutive modelling

Using the classical constitutive modelling method, it is easy to obtain the relationships of $\ln\dot{\varepsilon} - \ln\sigma$, $\ln\dot{\varepsilon} - \sigma$, $\ln\dot{\varepsilon} - \ln[\sinh(\alpha\sigma]$ and $\ln[\sinh(\alpha\sigma] - 1000/T$ which are shown in Figures 6(a), 6(b), 6(c) and 6(d), respectively.

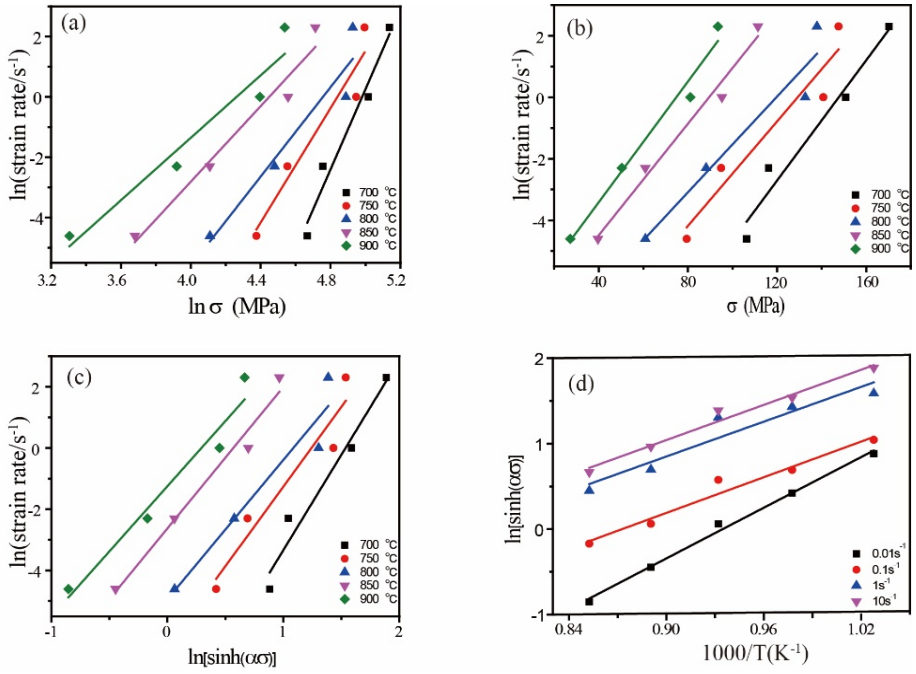

Figure 6: Relationships between various variables. (a) $\ln\dot{\varepsilon} - \ln\sigma$; (b) $\ln\dot{\varepsilon} - \sigma$; (c) $\ln\dot{\varepsilon} - \ln[\sinh(\alpha\sigma)]$; (d) $\ln[\sinh(\alpha\sigma)] - 1000/T$.

When the true strain is 0.2, the values of α, n, Q and A can be fitted to be 0.018, 4.97, –315091 J/mol, 2.63×10^{13} respectively. Assuming the values of n, Q and A are constant, the values of α can calculated and listed in Table 1 at different strain stages. When plotting the values of α against those corresponding strain ε values in Figure 7, it shows an exponential relationship which is fitted by,

$$\alpha = \exp(-3.915 - 0.573\varepsilon) \tag{7}$$

Table 1: Calculated values of α at different strain stages.

ε	0.2	0.3	0.4	0.5	0.6	0.7	0.8
α	0.0180	0.0168	0.0156	0.0148	0.0141	0.0134	0.0128

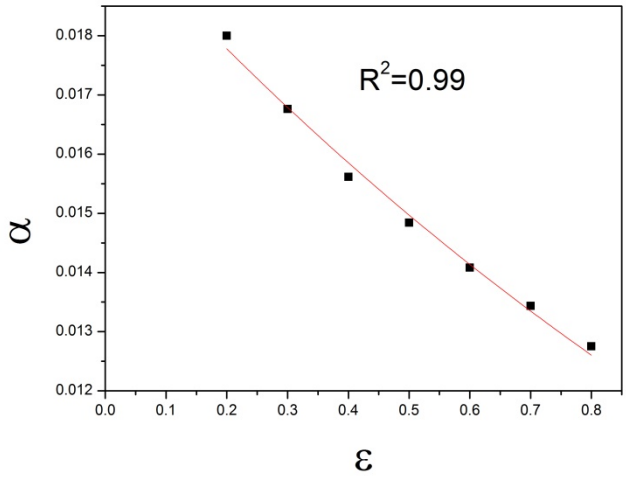

Figure 7: Fitting of the relationship between α and ε.

Thus a constitutive equation can be formed using these parameter values,

$$\dot{\varepsilon} = 2.63 \times 10^{13}\{\sinh[\exp(-3.915 - 0.573\varepsilon)\,\sigma]\}^{4.971}\exp(-\frac{315091}{RT}) \tag{8}$$

The calculated flow curves are then compared to the experimental ones as shown in Figure 8. A good consistency can be found by calculating the correlation coefficient R^2=0.96 in Figure 9.

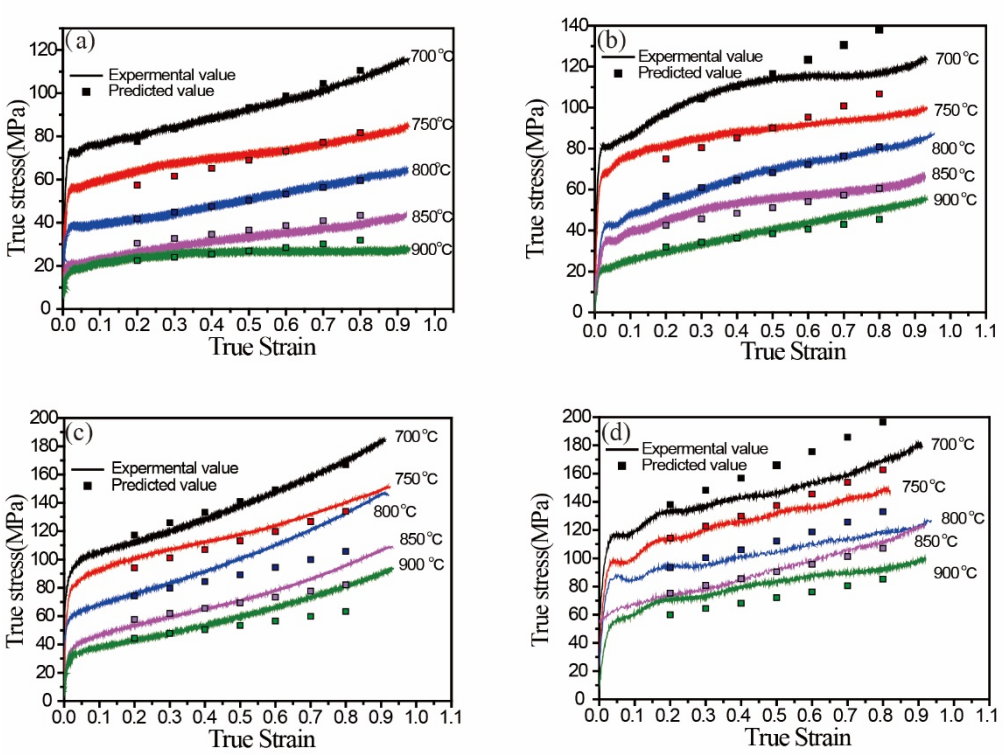

Figure 8: Comparison of the calculated and experimental flow stress curves of the Cu-Cr-Zr-Ti alloys at different strain rates. (a) 0.01 s^{-1}; (b) 0.1 s^{-1}; (c) 1 s^{-1}; (d) 10 s^{-1}.

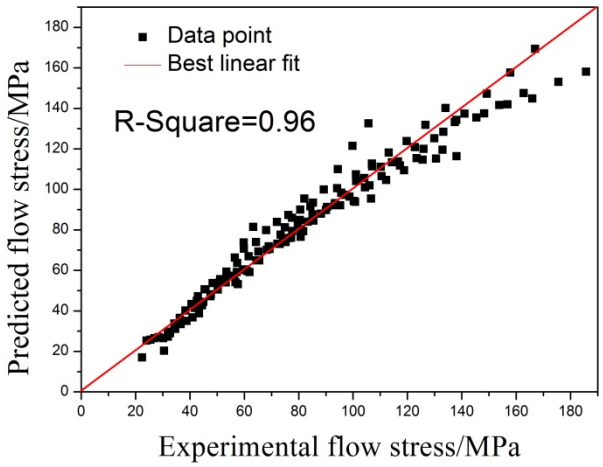

Figure 9: The calculation of correlation coefficients between predicted and experimental flow stress of Cu-Cr-Zr-Ti alloy.

5. Discussion

5.1 Model validation

In order to validate the model proposed in the present work, isothermal compression experiments have been carried out for Cu-Cr-Mg and Cu-Cr-Sn alloys. Equation (8) is used to predict the deformation behaviours and compared to the experimental results as shown in Figures 10 and 11, respectively. The calculation of correlation coefficients (0.97 for both Cu-Cr-Mg and Cu-Cr-Sn alloys) is presented in Figures 12 and 13. Previous work on the Cu-Cr-In alloy[29] has been used for validation as well and the correlation coefficient R^2=0.96 in Figure 14. This new proposed model has been applied to more alloys using available data from the literature. Very good agreement has been achieved for the correlation coefficients, with corresponding R^2 values all no less than 0.95 (please refer to the Appendix for more details).

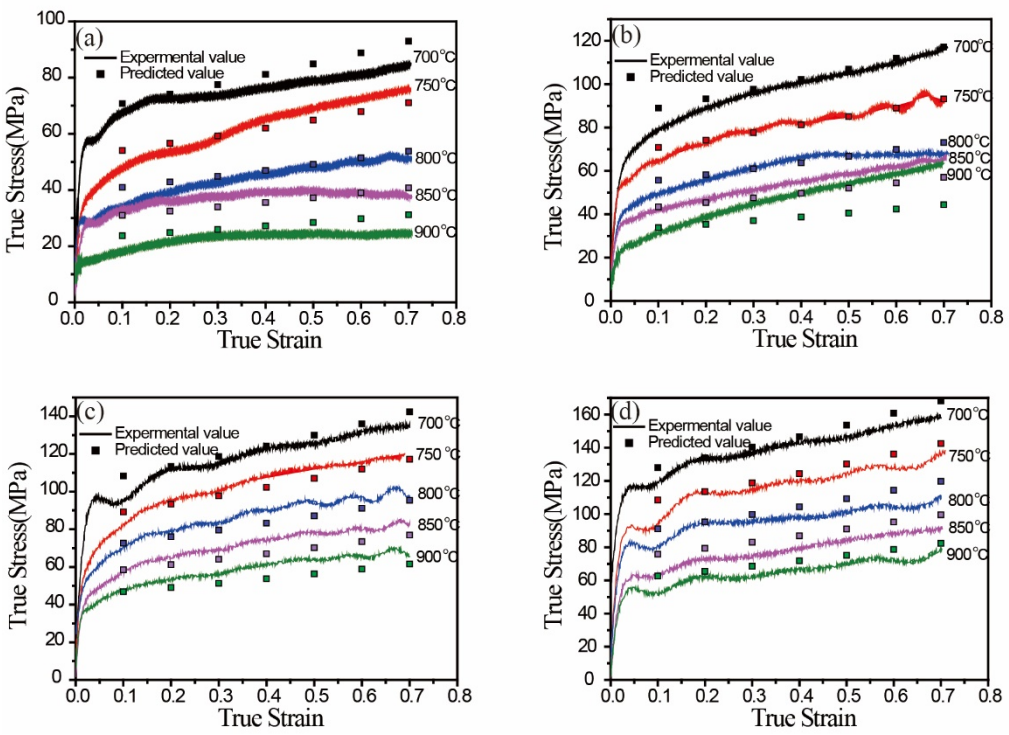

Figure 10: Comparison of the calculated and experimental flow stress curves of the Cu-Cr-Mg alloys at different strain rates. (a) 0.01 s^{-1}; (b) 0.1 s^{-1}; (c) 1 s^{-1}; (d) 10 s^{-1}.

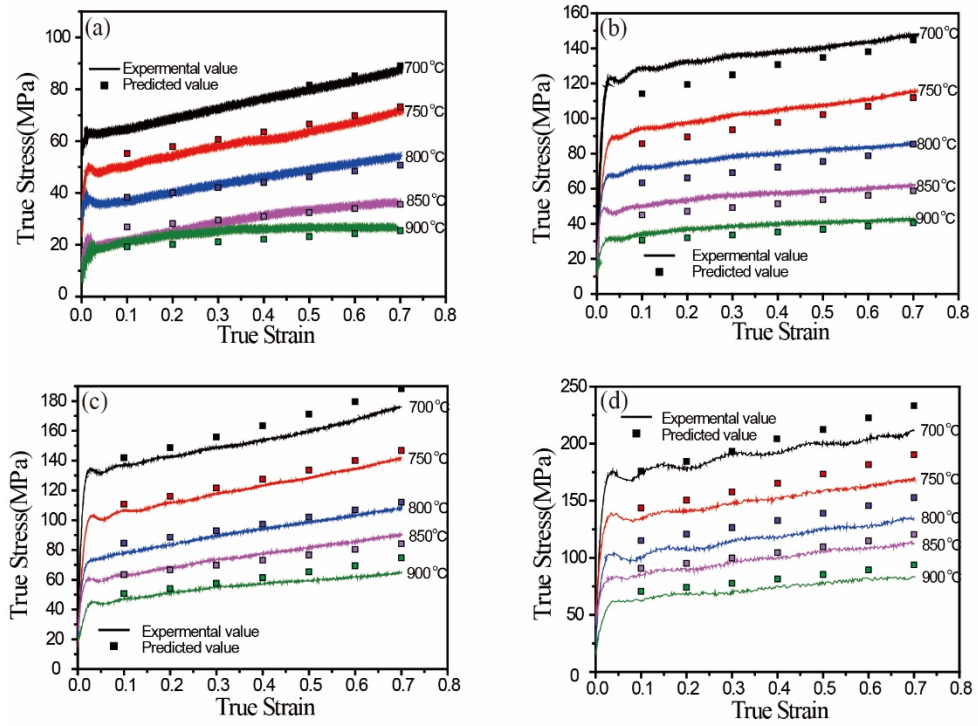

Figure 11: Comparison of the calculated and experimental flow stress curves of the Cu-Cr-Sn alloys at different strain rates. (a) 0.01 s^{-1}; (b) 0.1 s^{-1}; (c) 1 s^{-1}; (d) 10 s^{-1}.

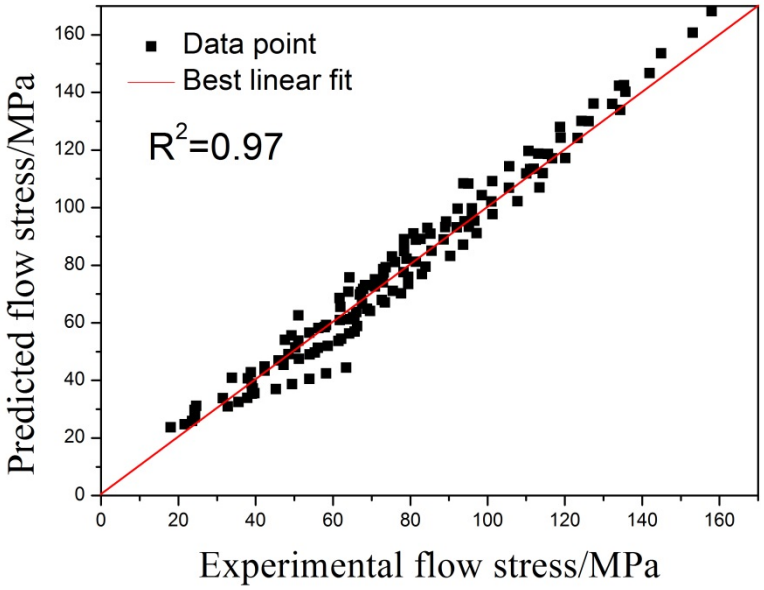

Figure 12: The calculation of correlation coefficients between predicted and experimental flow stress of Cu-Cr-Mg alloy.

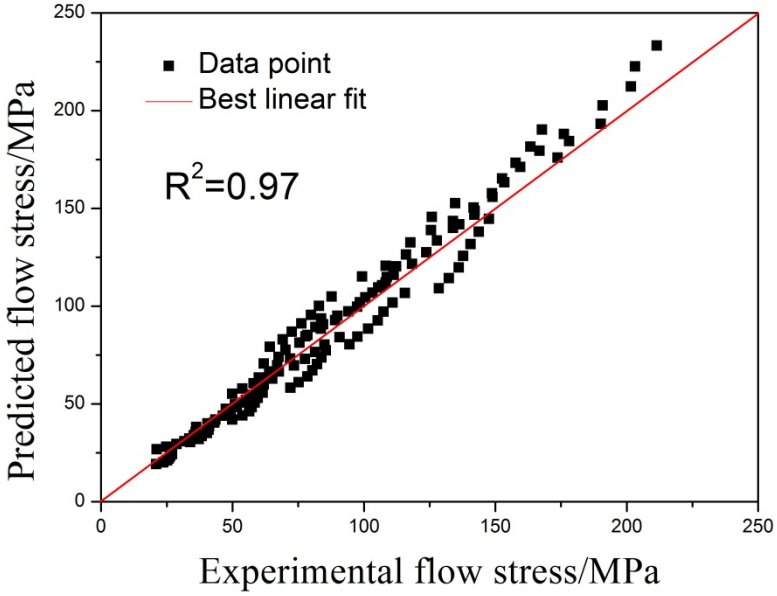

Figure 13: The calculation of correlation coefficients between predicted and experimental flow stress of Cu-Cr-Sn alloy.

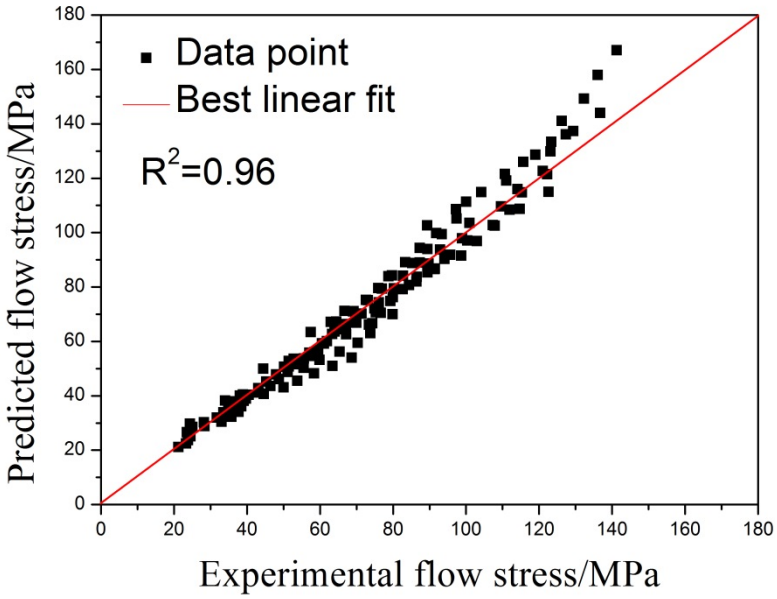

Figure 14: The calculation of correlation coefficients between predicted and experimental flow stress of Cu-Cr-In alloy[29].

5.2 Sensitivity study

When fitting the equation between the parameter α and true strain ε, the exponential function has been chosen. The model uses a linear relationship to check the sensitivity of the fitted equation. Figure 15 shows the fitting of predicted and experimental flow stress of the Cu-Cr-Zr-Ti alloy if a linear relationship is applied. The correlation coefficient falls from 0.96 to 0.94.

Moreover, if another parameter instead of α is chosen to reflect the effective stress (deduction of back stress from total stress), such as A, Q, or n, the flow curves cannot be reproduced well as shown in Figures 16 – 18.

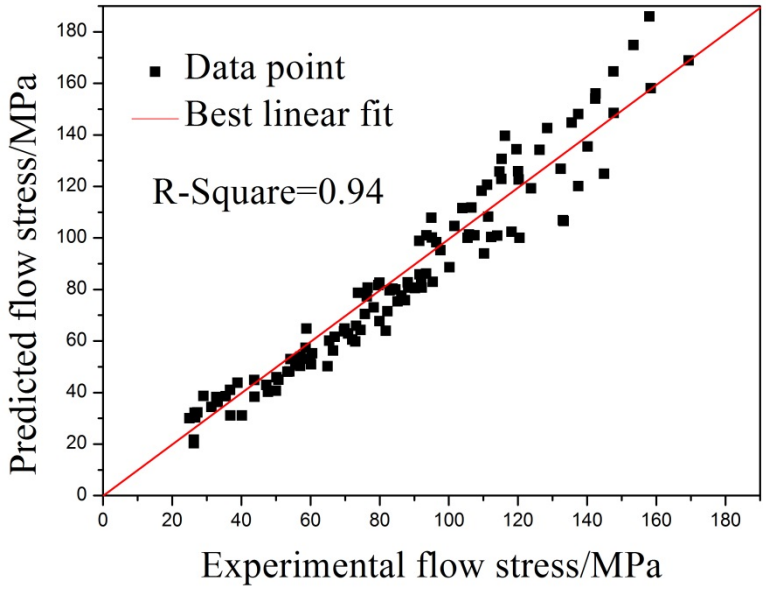

Figure 15: The calculation of correlation coefficients between predicted and experimental flow stress of Cu-Cr-Zr-Ti alloys using a linear relationship fitting.

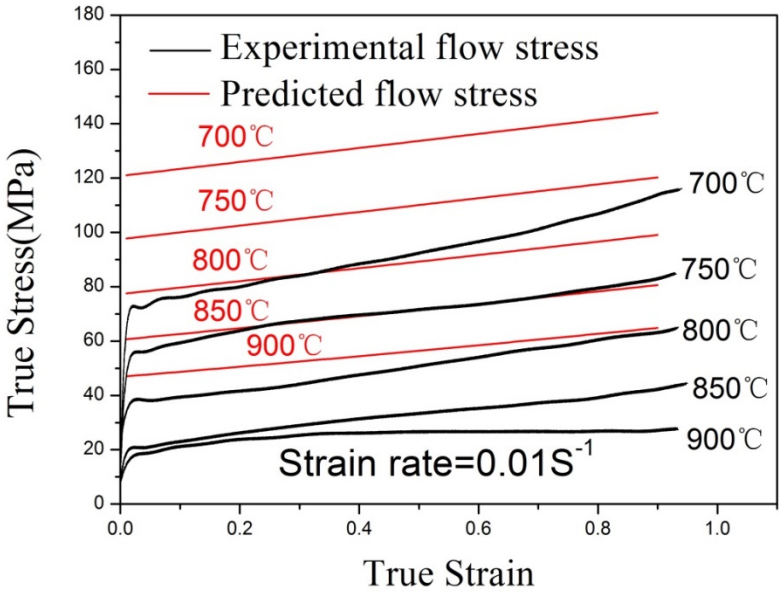

Figure 16: Comparison between predicted and experimental true stress versus true strain using *A* as a factor reflecting the effective stress.

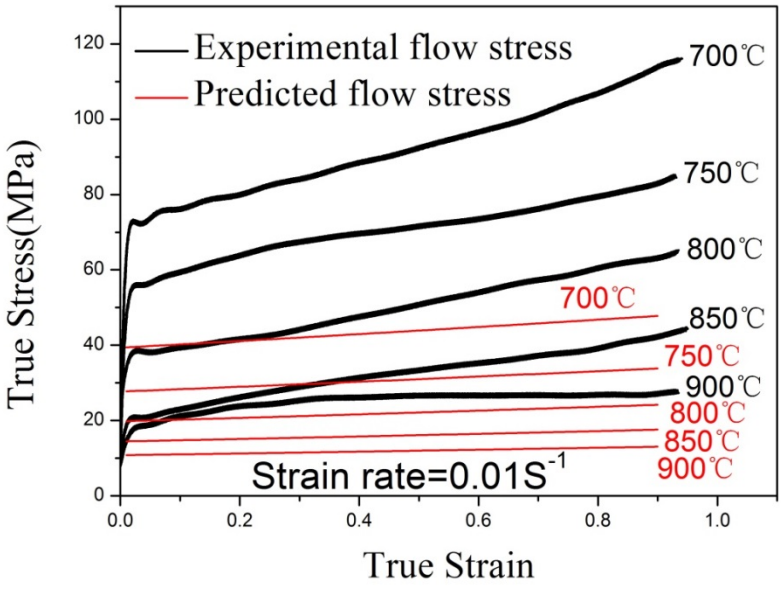

Figure 17: Comparison between predicted and experimental true stress versus true strain using Q as a factor reflecting the effective stress.

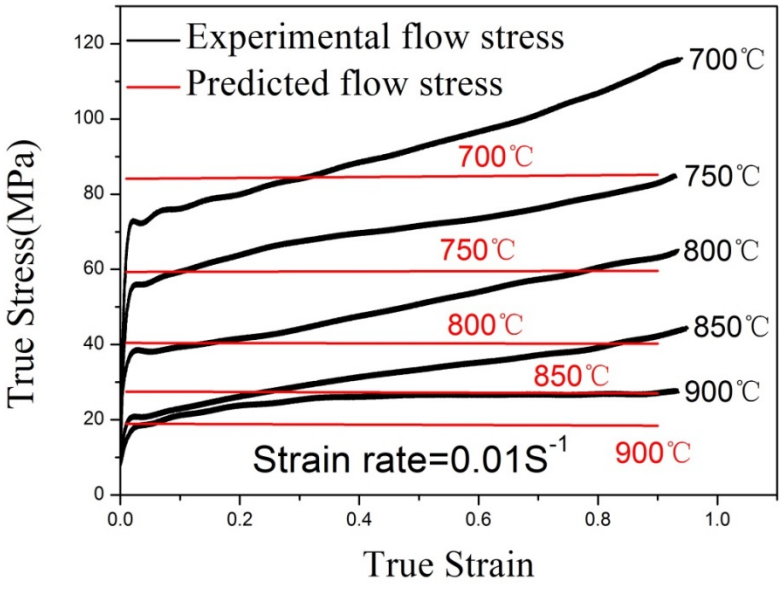

Figure 18: Comparison between predicted and experimental true stress versus true strain using n as a factor reflecting the effective stress.

5.3 Physical meaning of α

As was assumed, the parameter α should represent the proportion of effective stress after deducting the back stress, to the total stress,

$$\alpha = \frac{\sigma_{\text{eff}}}{\sigma} = \frac{\sigma_{\text{eff}}}{\sigma_{\text{eff}}+\sigma_{\text{back}}} \quad (9)$$

where σ_{eff} and σ_{back} are effective stress and back stress, respectively. This means that α is dependent upon the back stress. Back stress is a physical variable which can be described by dislocation density. During the compression process, as shown in the TEM results of Fig. 3, the dislocation density increases, while the estimation results based on XRD in Fig. 5 increase. Therefore, back stress during compression increases. At 700 °C, the change law of α value is shown in Figure 19, and the α value decreases with increasing strain. As shown in the TEM results at 900 °C in Figure 4, the dislocation density is almost constant, and the back stress remains constant during compression. The value of α varies slightly as shown in Figure 20. This is to say that the change of α value is consistent with the change of dislocation density. Therefore, we believe that α value depends on the back stress and is related to the dislocation density in the microstructure.

Although a qualitative explanation of the physical background for the parameter α is given, it remains difficult to calculate its value theoretically. In other words, it still remains unclear why an exponential function fits the parameter α, and how the values of a and b can be estimated from experimental determination or theoretical calculation. Nevertheless it gives a very interesting objective for the future work.

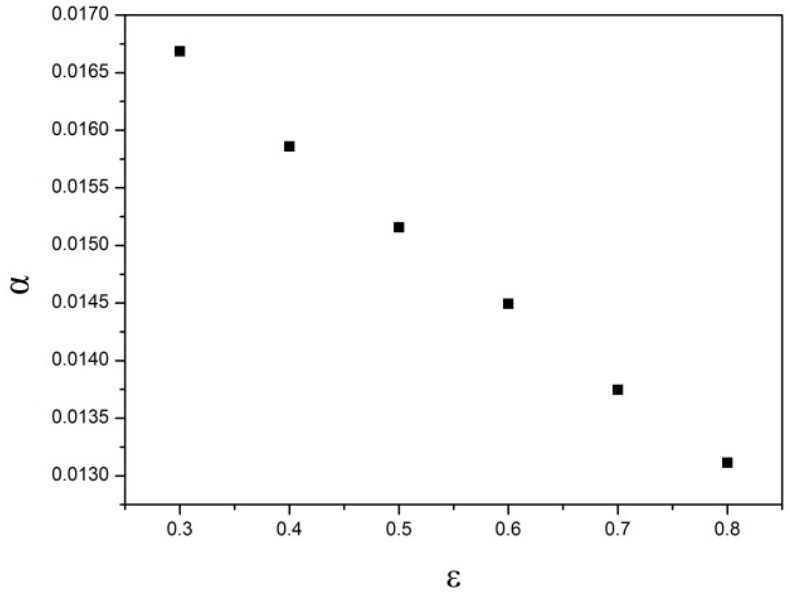

Figure 19: Relationship between α value and strain at 700 °C and $0.01S^{-1}$

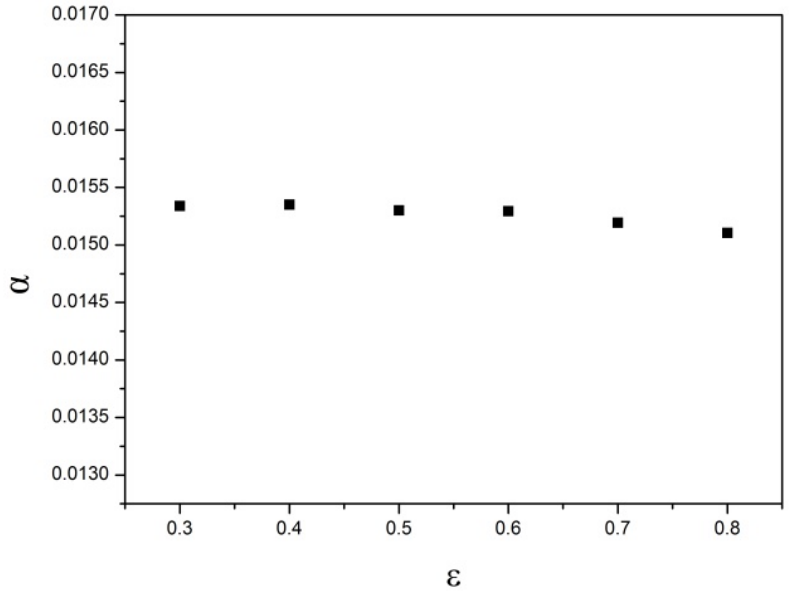

Figure 20: Relationship between α value and strain at 900 °C and $0.01S^{-1}$

6. Conclusions

A practical semi-empirical constitutive model has been proposed for strain hardening alloys during isothermal compression. Only four parameters are required to be fitted to reproduce the flow curves, including a new parameter α, which is given to reflect the effective stress (the part of total stress by taking away the back stress). The physical meaning of the parameter α is proven by XRD and TEM results. This method provides an easily implemented practical way of constitutive modelling for strain hardening alloys which combines both physically-based background understanding, and phenomenological-based methodology.

Acknowledgements

The authors would like to thank Dr. Haigen Wei, Dr. Weibin Xie and Mr. Qiqi Hao for his help during the course of experiments.

Funding

This work was supported by the National Key Research and Development Program of China (Grant No. 2016YFB0301400); the Department of Science and Technology of Jiangxi Province (Grant No. 20192ACBL21012); The Youth Jinggang Scholars Program in Jiangxi Province; and Ganzhou Talents Program.

Declaration of competing interest

The authors declare that they have no known competing financial interests or personal relationships that could have appeared to influence the work reported in this paper.

Appendix

The model proposed in the present work has been applied into other alloy systems in the literatures. Hereby we give some examples such as copper (Figures A1 and A2), steel (Figures A3 – A6), titanium (Figures A7 and A8) and magnesium (Figures A9 and A10). The corresponding data resources are listed with the figure captions for information.

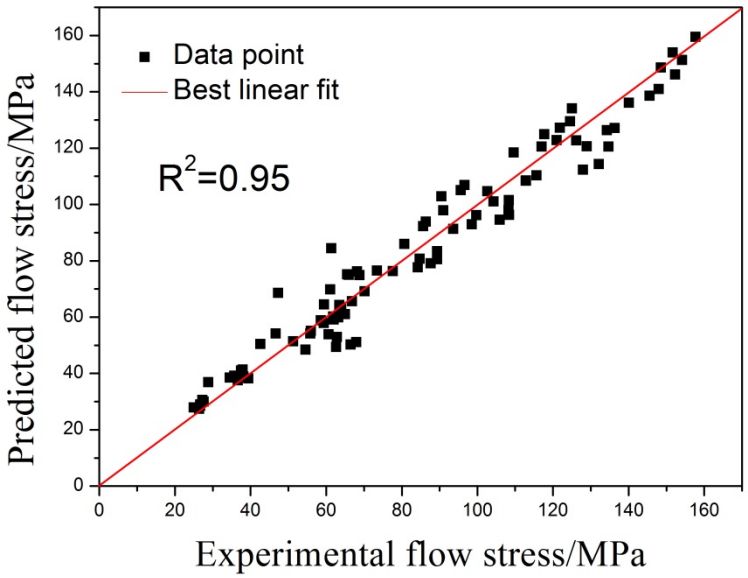

Figure A1: The calculation of correlation coefficients between predicted and experimental flow stress of Cu-Ni-Si-P alloy [37] using a constitutive equation $\dot{\varepsilon} = 4.62 \times 10^{23}\{\sinh[\exp(-3.994 - 0.177\varepsilon)\,\sigma]\}^{7.06}\exp(-\frac{485600}{RT})$.

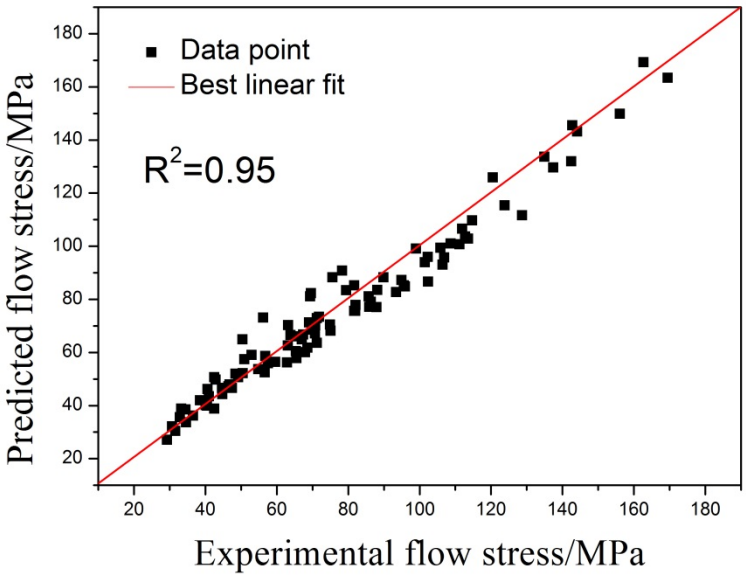

Figure A2: The calculation of correlation coefficients between predicted and experimental flow stress of Cu-Ni-Si-P alloy[28] using a constitutive equation $\dot{\varepsilon} = 3.01 \times 10^{15}\{\sinh[\exp(-4.000 - 0.380\varepsilon)\,\sigma]\}^{7.58}\exp(-\frac{370855}{RT})$.

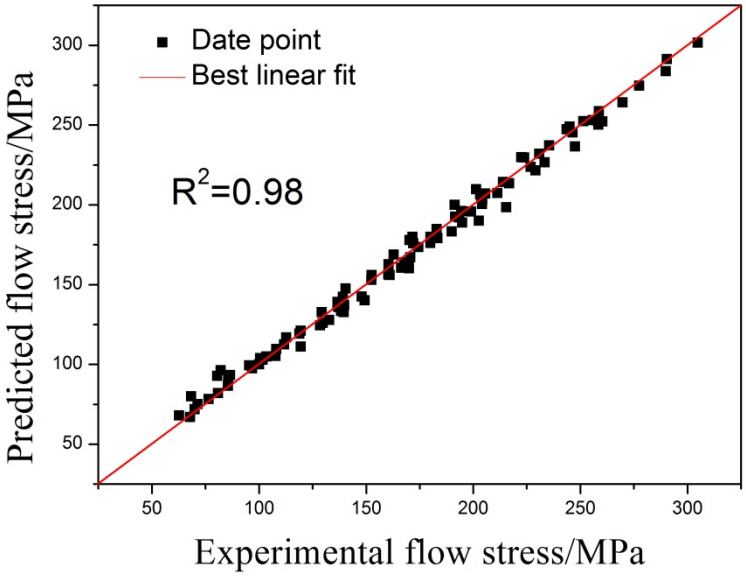

Figure A3: The calculation of correlation coefficients between predicted and experimental flow stress of CLAM steel[26] using a constitutive equation $\dot{\varepsilon} = 1.21 \times 10^{18}\{\sinh[\exp(-4.860 - 0.315\varepsilon)\,\sigma]\}^{7.91}\exp(-\frac{455280}{RT})$.

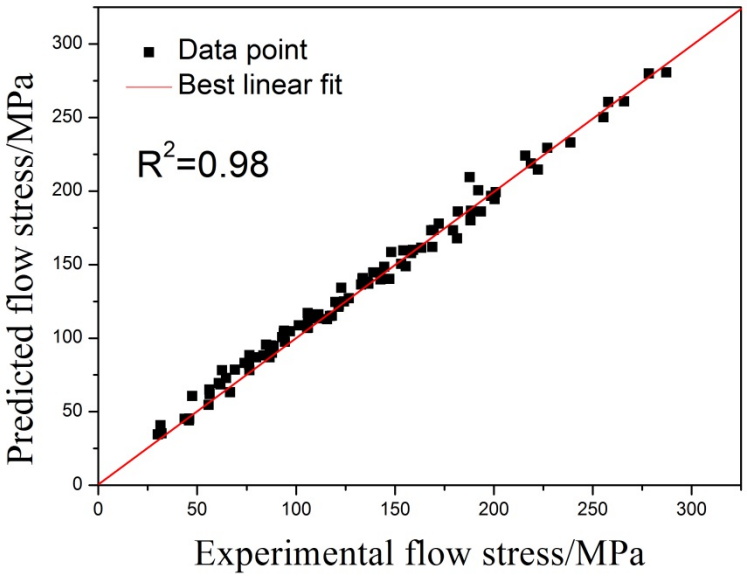

Figure A4: The calculation of correlation coefficients between predicted and experimental flow stress of P91 steel[38] using a constitutive equation $\dot{\varepsilon} = 2.69 \times 10^{16}\{\sinh[\exp(-4.656 - 0.420\varepsilon)\,\sigma]\}^{6.84}\exp(-\frac{449053}{RT})$.

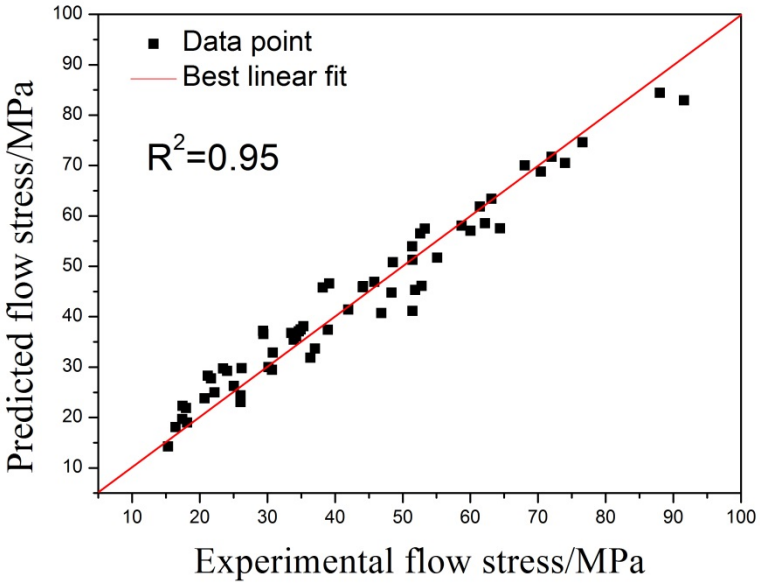

Figure A5: The calculation of correlation coefficients between predicted and experimental flow stress of 20CrMo steel[39] using a constitutive equation $\dot{\varepsilon} = 5.09 \times 10^{9}\{\sinh[\exp(-3.345 - 2.416\varepsilon)\,\sigma]\}^{3.80}\exp(-\frac{298247}{RT})$.

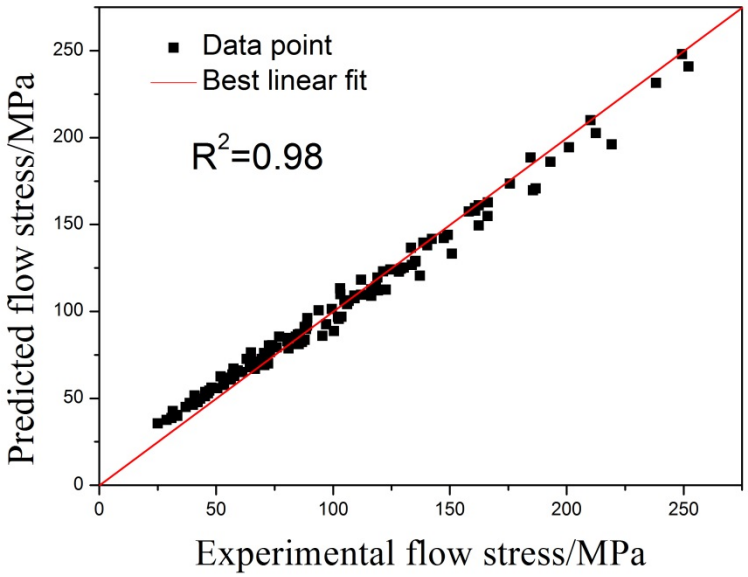

Figure A6: The calculation of correlation coefficients between predicted and experimental flow stress of 28CrMnMoV steel[40] using a constitutive equation $\dot{\varepsilon} = 7.95 \times 10^{18}\{\sinh[\exp(-4.431 - 0.313\varepsilon)\,\sigma]\}^{7.59}\exp(-\frac{510880}{RT})$.

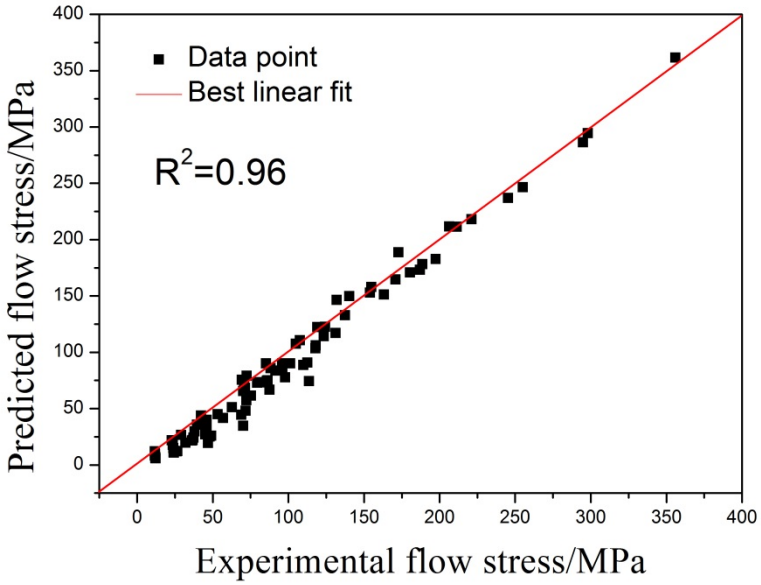

Figure A7: The calculation of correlation coefficients between predicted and experimental flow stress of Ti-6246S alloy[41] using a constitutive equation $\dot{\varepsilon} = 1.05 \times 10^{30}\{\sinh[\exp(-5.172 + 1.351\varepsilon)\,\sigma]\}^{3.85}\exp(-\frac{697648}{RT})$.

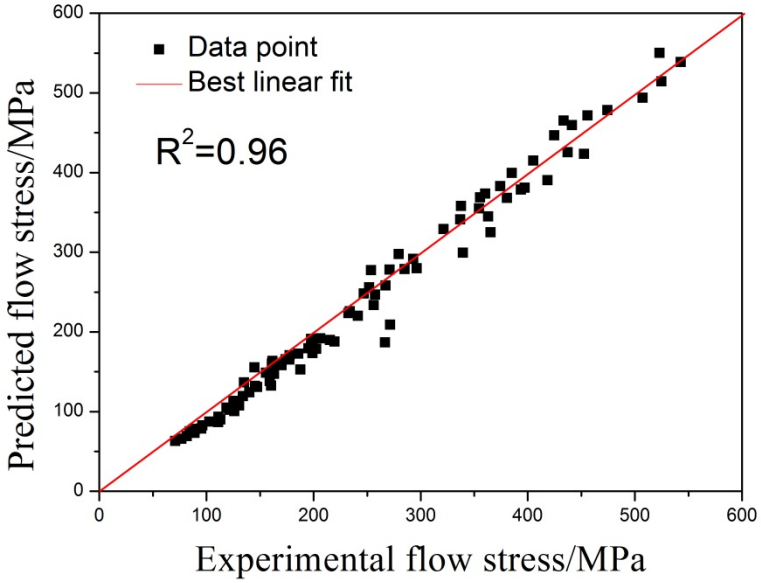

Figure A8: The calculation of correlation coefficients between predicted and experimental flow stress of Ti-Al alloy[42] using a constitutive equation $\dot{\varepsilon} = 6.64 \times 10^{14}\{\sinh[\exp(-5.392 + 0.521\varepsilon)\,\sigma]\}^{3.76}\exp(-\frac{438477}{RT})$.

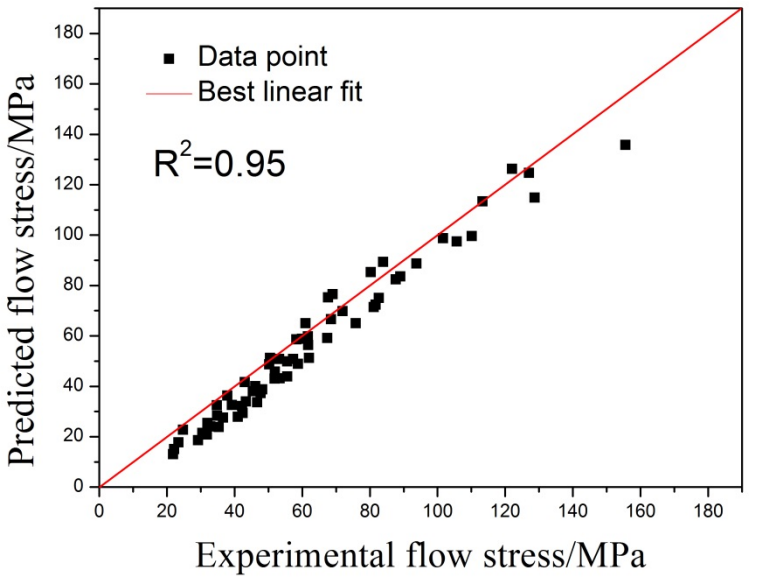

Figure A9: The calculation of correlation coefficients between predicted and experimental flow stress of AZ41 Mg alloy[18] using a constitutive equation $\dot{\varepsilon} = 2.30 \times 10^{11}\{\sinh[\exp(-5.159 + 2.048\varepsilon)\,\sigma]\}^{4.83}\exp(-\frac{141869}{RT})$.

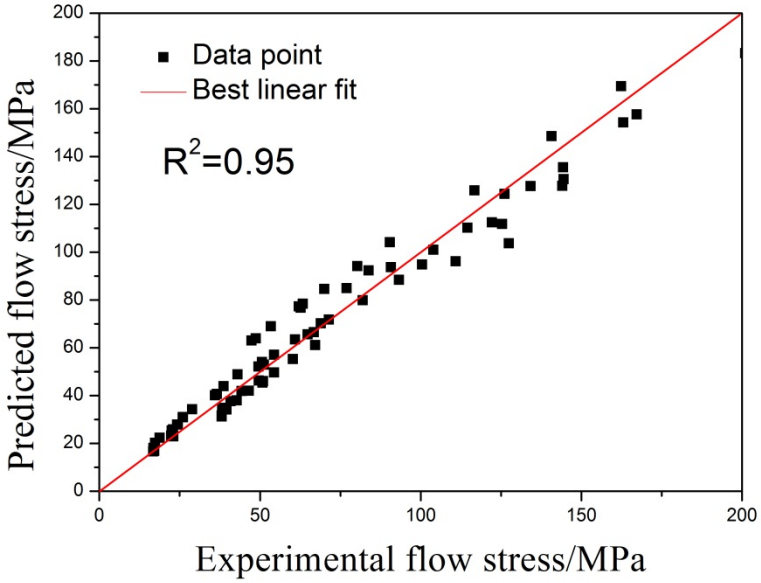

Figure A10: The calculation of correlation coefficients between predicted and experimental flow stress of Mg-6Al-1Zn alloy[1] using a constitutive equation $\dot{\varepsilon} = 7.00 \times 10^{17}\{\sinh[\exp(-4.169 + 0.751\varepsilon)\,\sigma]\}^{6.72}\exp(-\frac{248192}{RT})$.

Reference

[1] Y.C. Lin, X.M. Chen, A critical review of experimental results and constitutive descriptions for metals and allo.ys in hot working, Materials & Design 32 (2011) 1733-1759.

[2] G.R. Johnson, W.H. Cook, A constitutive model and data for metals subjected to large strains, high strain rates and high temperatures. In: Proceedings of the 7th International Symposium on Ballistics. Den Haag, The Netherlands; (1983) 541-543.

[3] A.S. Khan, S. Huang, Experimental and theoretical study of mechanical behavior of 1100 aluminum in the strain rate range 10^{-5}—10^{4} s^{-1}, International Journal of Plasticity, 8 (1992) 397-424.

[4] A.S. Khan, H.Y. Zhang, L. Takacs, Mechanical response and modeling of fully compacted nanocrystalline iron and copper, International Journal of Plasticity, 16 (2000) 1459-1476.

[5] A.S. Khan, Y.S. Suh, R. Kazmi, Quasi-static and dynamic loading responses and constitutive modeling of titanium alloys, International Journal of Plasticity, 20 (2004) 2233-2248.

[6] A.S. Khan, Y.S. Suh, X. Chen, L. Takacs, H.Y. Zhang, Nanocrystalline aluminum and iron: mechanical behavior at quasi-static and high strain rates, and constitutive modelling, International Journal of Plasticity, 22 (2006) 195-209.

[7] B. Farrokh and A.S. Khan, Grain size, strain rate, and temperature dependence of flow stress in ultra-fine grained and nanocrystalline Cu and Al: synthesis, experiment, and constitutive modelling, International Journal of Plasticity, 25 (2009) 715-732.

[8] Y.C. Lin, M.-S. Chen, J. Zhong, Constitutive modelling for elevated temperature flow behaviour of 42CrMo steel, Computational Materials Science, 42 (2008) 470-477.

[9] A.Yu. Churyumov, M.G. Khomutov, A.N. Solonin, A.V. Pozdniakov, T.A. Churyumova, B.F. Minyaylo, Hot deformation behaviour and fracture of 10CrMoWNb ferritic–martensitic steel, Materials & Design, 74 (2015) 44-54.

[10] D. Samantaray, S. Mandal, A.K. Bhaduri, Constitutive analysis to predict high-temperature flow stress in modified 9Cr–1Mo (P91) steel, Materials & Design， 31 (2010) 981-984.

[11] G.J. Chen, L. Chen, G.Q. Zhao, C.S. Zhang, W.C. Cui, Microstructure analysis of an Al-Zn-Mg alloy during porthole die extrusion based on modeling of constitutive equation and dynamic recrystallization, Journal of Alloys and Compounds, 710 (2017) 80-91.

[12] Y.Y. Dong, C.S. Zhang, G.Q. Zhao, Y.J. Guan, A.J. Gao, W.C. Sun, Constitutive equation and processing maps of an Al–Mg–Si aluminum alloy: Determination and application in simulating extrusion process of complex profiles, Materials & Design, 92 (2016) 983-997.

[13] C.-L. Gan, K.-H. Zheng, W.-J. Qi, M.-J. Wang, Constitutive equations for high temperature flow stress prediction of 6063 Al alloy considering compensation of strain, Transactions of Nonferrous Metals Society of China, 24 (2014) 3486-3491.

[14] Q.G. Meng, C.G. Bai, D.S. Xu, Flow behavior and processing map for hot deformation of ATI425 titanium alloy, Journal of Materials Science & Technology, 34

(2018) 679-688.

[15] Y.-H. Xiao, C. Guo, X.-Y. Guo, Constitutive modeling of hot deformation behavior of H62 brass, Materials Science and Engineering A, 528 (2011) 6510-6518.

[16] F.-C. Ren, J. Chen, F. Chen, Constitutive modeling of hot deformation behavior of X20Cr13 martensitic stainless steel with strain effect, Transactions of Nonferrous Metals Society of China, 24 (2014) 1407-1413.

[17] W.J. Kim T.Y. Kwak, Constitutive modeling and understanding of the hot compressive deformation of Mg-9.5Zn-2.0Y magnesium alloy with reduced number of strain-dependent constitutive parameters, Metals and Materials International, 23 (2017) 660-672.

[18] Z.W. Cai, F.X. Chen, J.Q. Guo, Constitutive model for elevated temperature flow stress of AZ41M magnesium alloy considering the compensation of strain, Journal of Alloys and Compounds, 648 (2015) 215-222.

[19] J.P. Li, X.S. Xia, Modeling high temperature deformation behavior of large-scaled Mg-Al-Zn magnesium alloy fabricated by semi-continuous casting, Journal of Materials Engineering and Performance, 24 (2015) 3539-3548.

[20] P.M. Souza, H. Beladi, R.P. Singh, P.D. Hodgson, B. Rolfe, An analysis on the constitutive models for forging of Ti6Al4V alloy considering the softening behavior, Journal of Materials Engineering and Performance, 27 (2018) 3545-3558.

[21] F. Pilehva, A. Zarei-Hanzaki, M. Ghambari, H.R. Abedi, Flow behavior modelling of a Ti-6Al-7Nb biomedical alloy during manufacturing at elevated temperatures, 51 (2013) 457-465.

[22] Y.X. Wang, G.Q. Zhao, X. Xu, X.X. Chen, C.S. Zhang, Processing map establishment and microstructure analysis of spray deposited Al-Cu-Li alloy 2195, Journal of Alloys and Compounds, 779 (2019) 735-751.

[23] Z.M. Cai, H.C. Ji, W.C. Pei, X.F. Tang, X.M Huang, J.P. Liu, Hot workability, constitutive model and processing map of 3Cr23Ni8Mn3N heat resistant steel, Vacuum, 165 (2019) 324-336.

[24] Y. Cao, H.S. Di, R.D.K. Misra, X. Yi, J.C. Zhang, T.J. Ma, On the hot deformation behavior of AISI 420 stainless steel based on constitutive analysis and CSL model, Materials Science and Engineering A, 593 (2014) 111-119.

[25] M.H. Wang, K. Wei, X.J. Li, A.Z. Tu, Constitutive modeling for high temperature flow behavior of a high-strength manganese brass, Journal of Central South University, 25 (2018) 1560-1572.

[26] W.-T. Wang, W.-Z. Guo, B. Huang, J. Tao, H.-G. Li, W.-J. Pei, The flow behaviors of CLAM steel at high temperature, Materials Science and Engineering A, 599 (2014) 134-140.

[27] Y. Zhang, H.L. Sun, A.A. Volinsky, B.H. Tian, K.X. Song, B.J. Wang, Y. Liu, Hot workability and constitutive model of the Cu-Zr-Nd alloy, Vacuum, 146 (2017) 35-43.

[28] J. Cai, K.S. Wang, C.P. Miao, W.B. Li, W. Wang, J. Yang, Constitutive analysis to predict high-temperature flow behavior of BFe10-1-2 cupronickel alloy in consideration of strain, Materials & Design, 65 (2015) 272-279.

[29] H.M. Chen, P.Z. Gao, H.C. Peng, H.G. Wei, W.B. Xie, H. Wang, B. Yang, Study on the hot deformation behavior and microstructure evolution of Cu-Cr-In alloy,

Journal of Materials Engineering and Performance, 28 (2019) 2128-2136.

[30] Q. Liu, X. Zhang, Y. Ge, Effect of processing and heat treatment on behavior of Cu–Cr–Zr alloys to railway contact wire, Metallurgical and Materials Transactions. A, 37 (2006) 3233-3238.

[31] C.D. Xia, Y.L. Jia, W. Zhang, Study of deformation and aging behaviors of a hot rolled-quenched Cu-Cr-Zr-Mg-Si alloy during thermo mechanical treatments, Materials and Design, 39 (2012) 404-409.

[32] K. Wang, K.F. Liu, J.B. Zhang, Microstructure and properties of aging Cu–Cr–Zr alloy, Rare Metals, 33 (2014) 134-138.

[33] Y. Pang, C.D. Xia, M.P. Wang, Effects of Zr and (Ni, Si) additions on properties and microstructure of Cu-Cr alloy, Journal of Alloys and Compounds, 582 (2014) 786-792.

[34] K. Mihara, T. Takeuchi, H.G. Suzuki, Effect of Zr on Aging Characteristics and Strength of Cu-Cr in situ Composite, Journal of the Japan Institute of Metals, 62 (1998) 238-245.

[35] F. Jiang, X.B. Cheng, M. Cheng, Research progress on nano-precipitated phases of high-strength and high-conductivity Cu-Cr-Zr system a and their mechanisms (in Chinese), Materials Reports, 23 (2009) 72-76.

[36] G.K. Williamson, W.H. Hall, X-ray line broadening from field aluminium and wolfram, Acta Metallurgica, 1 (1953) 22-31.

[37] Y. Zhang, P. Liu, B.-H. Tian, Y. Liu, R.-Q. Li, Q.-Q. Xu, Hot deformation behavior and processing map of Cu-Ni-Si-P alloy, Transactions of Nonferrous Metals

Society of China (English Edition), 23 (2013) 2341-2347.

[38] K. Deng, Y.T. Li, J.H. Fu, Q. Liu, High temperature rheological behavior and constitutive equation of as-cast heat-resisting alloy steel P91 (in Chinese), Forging & Stamping Technology, 40 (2015) 100-106.

[39] A. He, G.L. Xie, H.L. Zhang, X.T. Wang, A comparative study on Johnson-Cook, modified Johnson-Cook and Arrhenius-type constitutive models to predict the high temperature flow stress in 20CrMo alloy steel, Materials & Design, 52 (2013) 677-685.

[40] H.-Y. Li, Y.-H. Li, X.-F. Wang, J.-J. Liu, Y. Wu, A comparative study on modified Johnson Cook, modified Zerilli–Armstrong and Arrhenius-type constitutive models to predict the hot deformation behavior in 28CrMnMoV steel, Materials & Design, 49 (2013) 493-501.

[41] A. Hajari, M. Morakabati, S.M. Abbasi, H. Badri, Constitutive modeling for high-temperature flow behavior of Ti-6242S alloy, Materials Science and Engineering A, 681 (2017) 103-113.

[42] X.-P. Liang, Y. Liu, H.-Z. Li, C.-X. Zhou, G.F. Xu, Constitutive relationship for high temperature deformation of powder metallurgy Ti-47Al-2Cr-2Nb-0.2W alloy, Materials & Design, 37 (2012) 40-47.